

Contents lists available at [ScienceDirect](#)

Atmospheric Research

journal homepage: www.elsevier.com/locate/atmos

Assessment of biomass burnings activity with the synergy of sunphotometric and LIDAR measurements in São Paulo, Brazil

G.L. Mariano ^{a,*}, F.J.S. Lopes ^b, M.P.P.M. Jorge ^a, E. Landulfo ^b

^a Centro de Previsão de Tempo e Estudos Climáticos - CPTEC, Instituto Nacional de Pesquisas Espaciais – INPE, Rodovia Presidente Dutra, Km 40 - CEP: 12630-000, Cachoeira Paulista-SP, Brazil

^b Instituto de Pesquisas Energéticas e Nucleares – IPEN, Av. Lineu Prestes 2242, Cidade, Universitaria, CEP: 05508-000, São Paulo, SP, Brazil

ARTICLE INFO

Article history:

Received 3 June 2009

Received in revised form 21 May 2010

Accepted 26 August 2010

Available online xxx

Keywords:

LIDAR

Aerosol

Biomass burning

ABSTRACT

In the period of July–November of 2007 an aerosol profiling campaign was carried out with a backscattering LIDAR system in São Paulo, Brazil (23° 33'S, 46° 44'W). The goals of this campaign were to perform an aerosol long period observation in the lower atmosphere (up to 10 km) and extract correlations among the microphysical properties obtained from different platforms, as well to pinpoint events where strong indications of biomass burning plumes were present above the planetary boundary layer (PBL) and still impact quality reports emitted by ground stations provided by the local environmental agency. In this context the present study aims to investigate the impact that this type of aerosol has on the environment of São Paulo when active fires in South America are observed in close and remote areas. Besides the LIDAR system, an AERONET Sunphotometer was used to help in characterizing the aerosol optical properties. Ten cases were selected as an identification of biomass burning layer entrance and after they were confirmed by NOAA-12 AVHRR sensor and 5-day Hysplit generated backtrajectories. A statistical analysis was carried out for analysis of the extinction-to-backscattering ratio (LIDAR ratio – LR) together with the sunphotometer retrieved Angström Exponent (AE) and aerosol optical depth (AOD) data. The observed layer sources were potentially from remote regions as the South Amazon basin and the north portion of Argentina and closer parts of São Paulo state related to sugar cane harvesting activities. The biomass burning plume heights were between 3 and 8 km. It has been found that LR, AE and AOD values ranged from 44 to 147 sr, from 0.85 to 1.58 and from 0.14 to 0.53, respectively. In a case study for September 7, 2007, an air mass with influence of biomass burning reached the city of São Paulo leading to a LR of 59 sr. Despite the AOD value of 0.33, the aerosol size distribution analysis showed a higher amount of fine particulate matter in relation to coarse that is an indicative of transport of material in the free atmosphere. The analysis carried out in this study shows that these plumes affect greatly the LR mean values while with low effect on the AOD and AE daily averages.

© 2010 Elsevier B.V. All rights reserved.

1. Introduction

The direct radiative forcing estimated for biomass burning aerosols (in short form BBA) was revised due to their strong influence over the clouds (IPCC, Intergovernmental Panel on

Climate Change, 2007). Brazil has an important role in the biomass burning activity, according to CPTEC/INPE (www.cptec.inpe.br/queimadas), with the detection of approximately 100000 active fires in 2007. The biomass burning includes the kindling of forests, savannas, and agricultural land. In Brazil, specifically in the Northeast and Southeast regions where the harvesting of sugarcane is of great importance, the injection of aerosols are in certain instances due the fire setting of sugarcane crops in a programmed way.

* Corresponding author.

E-mail address: glauber.mariano@cptec.inpe.br (G.L. Mariano).

In the last decades a great number of studies about BBA was carried out mainly on the physical direct – (IPCC, Intergovernmental Panel on Climate Change, 2001); Yamasoe et al., 1998; Yamasoe et al., 2000 and indirect effects – (Rosenfeld, 2000; Dias et al., 2004) and on chemical properties (Lara et al., 2001; Lara et al., 2005) and also biomass burning reviews were published (Reid et al., 2005a; Reid et al., 2005b). In terms of air quality, biomass burning is a major source of air pollution and the second largest source of anthropogenic aerosols (IPCC, Intergovernmental Panel on Climate Change, 2001), specifically in Brazil, it is possible to highlight several studies referring to: gases (Crutzen and Andreae, 1990; Kaufman and Tanré, 1998), trace gas transport (Boian and Kirchhoff, 2004), particulate matter composition (Kaufman and Tanré, 1998), effects on diffuse and photosynthetically active radiation (Yamasoe et al., 2006), cloud physics (Andreae et al., 2004), satellite measurements (Kaufman et al., 2002) and air mass trajectories (Freitas et al., 1996; Longo et al., 1998).

In several parts of the globe it is possible to pinpoint some efforts on research of biomass burning with LIDAR systems such as (Balis et al., 2003) who studied one episode of biomass burning using Raman LIDAR and sunphotometer in Greece with high aerosol optical depth values. From the analysis of 4-day backtrajectories they showed some indication that these air masses were advected from Bulgaria and the northern coast of Black Sea, where fires occurred a few days earlier. The estimated mean extinction-to-backscatter ratios from the Raman LIDAR were 62 ± 8 sr for 0.8 to 4.5 km (smoke layer) at 355 nm and the calculated AE from a multi-filter rotating shadowband radiometer indicated the presence of small particles (by obtaining an Ångström Exponent (AE) of approximately 1.78). Amiridis et al. (2005) in the framework of the European Aerosol Research LIDAR Network (EARLINET) at Thessaloniki, Greece (40.5° N, 22.9° E) found that the 4-year (2001–2004) mean boundary layer particle optical depth at 355 nm was 0.44 ± 0.18 , and the total aerosol optical depth was 0.63 ± 0.27 . Amiridis et al. (2009) studied 10 cases of biomass burning during 2001–2005 in Europe (Russia and Eastern Europe) and transported to Greece. In this paper high AOD values were also identified with a UV–Raman LIDAR while AE ranged between 0.5 and 2.4 indicating a variety of particle sizes.

Noh et al. (2008), after analyzing 63 aerosol layers between 2004 and 2005 with focusing mainly in spring and autumn seasons, observed a high quantity of light absorbing material, which is believed to be generated by coal combustion and agricultural biomass burning. Evidence were found of aerosols from Siberian forest fires transported to the Korean peninsula in June, 2004, besides occasional measurements during spring were influenced by smoke aerosols transported from this region. The biomass burning particles identified in this study were detected above the PBL resulting from the long-range transport. The biomass burning particles could be easily separated from other sources (dust or anthropogenic pollution) due to the LIDAR ratio spectral behavior (higher LIDAR ratio at 532 nm than at 355 nm – 5–15 sr lower values at 355 nm than at 532 nm) and the relatively low Ångström Exponent values (0.93 ± 0.26). In order to track and discriminate different aerosol types, Basart et al. (2009) carried an analysis of 39 AERONET Mediterranean and African stations from 1994 to 2007, and introduced a graphical method developed by Gobbi et al. (2007). In this

study they observed an important contribution of biomass burning in the sub-Sahel region in winter. In this region, the aerosol type is dominated by dust, mostly in the dry season. However, it is possible to notice a second aerosol type which contributed to turbidity ($AOD > 1.5$) especially in late autumn–winter, coming from biomass burning aerosols emanating from the Savannah vegetation in Sudanian zone.

In Brazil, at the time of the campaign there were 2 LIDAR systems operating: the first one devoted to stratospheric studies (Clemesha and Rodrigues, 1971) and the other, an elastic backscatter LIDAR system, focus its studies in tropospheric aerosol profiling for air pollution applications (Landulfo et al., 2004). In Brazil, up to date, few studies using LIDAR were made concerning biomass burning. Landulfo et al. (2003) employed an elastic LIDAR showing the presence of highly absorbent particles, characteristic of biomass burning aerosol. In the present study four-day air mass backtrajectory analysis and satellite data showed that the aerosol could originate from the Amazon regions. The optical depth measured by the sunphotometer also indicated the presence of biomass burning coming from these distant regions. Despite the average value for LR around 45 sr (typical of urban environment), studies indicate that the presence of dust and biomass burning aerosol transported from great distances away from São Paulo City increases the suspended atmospheric aerosol variability where normally the layer between 1 and 3 km is responsible for 20–25% of all the tropospheric aerosol amount (Landulfo et al., 2005).

Herein a multi-instrument approach was employed, using active and passive remote sensors, namely a LIDAR system, sunphotometer (AERONET's CIMEL) and modelling using Hysplit and MODIS images plus NOAA's-12 active fire mask. The sunphotometer data are used to provide AOD values at selected wavelengths and also to derive the AE and aerosol size distribution values over São Paulo. This multi-instrumental approach can be extremely helpful to comprehend the scenery described above (Landulfo et al., 2005). Besides it will help in building a time series of these specific events which are not common nor easily detected in urban regions such a São Paulo. The LIDAR data were analyzed with the intention of finding aerosol layers suspected of being originated from biomass burning (highly absorbent material) confirmed with backtrajectories and NOAA-12 active fires plus MODIS images. In Section 2 of this paper a brief overview of the experimental setup of the LIDAR system, the CIMEL photometer and the Hysplit model will be given. Section 3 shows the data analysis and methodology for LIDAR data and AERONET data. In Section 4 some studies of aerosol LIDAR measurements will be analyzed and discussed, such as the possible origin regions with biomass burning activities through backtrajectories, physical (size distribution and AE) and optical (LR and AOD) characteristics of these particles through LIDAR and AERONET measurements. Also, a case study for September 7, 2007 was analyzed. Finally, Section 5 presents our concluding remarks.

2. Experimental setup

2.1. LIDAR system

A ground-based elastic backscatter LIDAR system is in operation since 2001 in the Environmental Laser Applications

Laboratory at the Centre for Laser and Applications (CLA) at the Instituto de Pesquisas Energéticas e Nucleares – IPEN in São Paulo University – USP. The Metropolitan area of São Paulo (MASP) and instrument locations in the São Paulo district area are depicted in Fig. 1 (point L).

The LIDAR technique is based on the emission of a collimated laser beam through the atmosphere and on the detection of the backscattered laser light by the suspended atmospheric aerosols and molecules. A backscattering LIDAR can thus provide information on the PBLs mixed layer depth, entrainment zones and convective cell structure, aerosol distribution, clear air layering, cloud-top altitudes, cloud statistics, atmospheric transport processes and other inferences of air motion (Ferrare et al., 1991; Mel et al., 1985; Crum et al., 1987; Balis et al., 2000).

The LIDAR system is a single-wavelength backscatter system pointing vertically to the zenith and operating in the coaxial mode. The light source is based on a commercial Nd:YAG laser (Brilliant by Quantel SA) operating at the second harmonic frequency (SHF), namely at 532 nm, with a fixed repetition rate of 20 Hz. The average emitted power can be selected up to values as high as 3.3 W. The emitted laser pulses have a divergence of less than 0.5 mrad. A 30 cm diameter telescope (focal length $f = 1.3$ m) is used to collect the backscattered laser light. The telescope's field of view (FOV) is variable (1–2 mrad) by using a small diaphragm. LIDAR is currently used with a fixed FOV of the order of 1 mrad, which according to geometrical calculations (Chourdakis et al., 2002) permits a full overlap between the telescope FOV and the laser beam at heights around 300 m above the LIDAR system. This FOV value, in accordance with the detection electronics, permits the probing of the atmosphere up to the free troposphere (12–15 km asl).

The backscattered laser radiation is then sent to a photomultiplier tube (PMT) coupled to a narrowband (1 nm full width at half maximum – FWHM) interference filter to assure the reduction of the solar background during daytime

operation and to improve the signal-to-noise ratio (SNR) at altitudes greater than 3 km. The PMT output signal is recorded by a Transient Recorder in both analog and photoncounting modes. Data are averaged between 2 and 5 min and then summed up over a period of about 1 h, with a typical spatial resolution of 15 m, which corresponds to a 100 ns temporal resolution. The observation period comprised a total of 67 days and LIDAR ratio data at 532 nm of which 41 days occurred in winter and 26 in spring.

2.2. AERONET Sun-tracking photometer

Besides the LIDAR, there was a co-located CIMEL sun-photometer which provides aerosol measurements to determine the AOD values at several wavelengths in the visible spectrum and thus to enable the assessment of the aerosol extinction values at the same spectral region. The CIMEL 318A spectral radiometer is a solar-powered weather-hardy robotically pointed sun and sky instrument. This instrument is installed on the roof of the Physics Department at the University of São Paulo (Fig. 1 point L). The principle of operation of the CIMEL instrument is to acquire aureole and sky radiance measurements. The standard measurements are taken 15 min apart, in order to allow cloud contamination checking. These measurements are taken in the whole spectral interval, and their number depends on daytime duration. The instrument precision and accuracy follow the standard Langley plot method within the standard employed by the AERONET network (Holben et al., 1998). The CIMEL sunphotometer is calibrated periodically by a remote computer or locally under the supervision of the AERONET network. The calibration methodology assures coefficient accuracy between 1 and 3%, nonetheless various instrumental, calibration, atmospheric, and methodological factors influence precision and accuracy, of optical depth and effectively the total uncertainty in the AOD retrieved values is less than 8% (Chourdakis et al., 2002). CIMEL data level 2.0

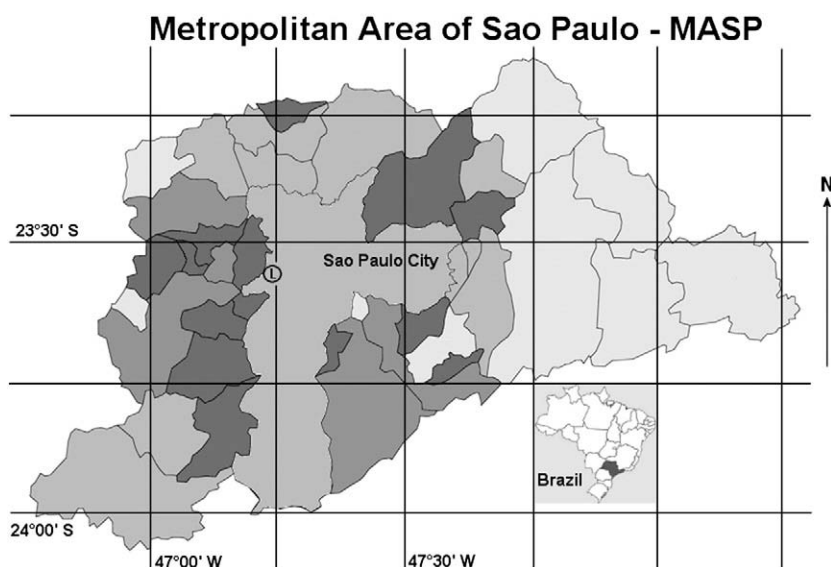


Fig. 1. São Paulo Metropolitan Region (MASP) map with the sampling locations indicated: (L) São Paulo University Campus (USP), site of the Backscatter LIDAR system and CIMEL, meteorological station.

were used in order to eliminate interference from clouds and have are quality-assured (Holben et al., 1998).

2.3. Hysplit model

Hysplit was designed by the Bureau of Meteorology of Australia and the ARL-NOAA of USA. Information on Hysplit can be obtained at <http://www.arl.noaa.gov/Hysplit.php>. Hysplit calculates advection, dispersion and deposition using either puff or particle approaches. The model uses all the available meteorological data for the whole domain placed in a 3D grid (Draxler and Hess, 1997).

There are many studies employing Hysplit backtrajectory analysis (Vana and Tamm, 2002; Gassmann and Pérez, 2006; McGowan and Clark, 2008). The trajectory from São Paulo City was simulated, on the instant and height where a possible plume was detected by LIDAR, using the Hysplit model. In this paper 120-h (five days) backtrajectories of air masses ending over the city of São Paulo were calculated, in order to have a more realistic input about the origin of the air masses ending over our LIDAR site and to locate the aerosols sources near the São Paulo region. The backward trajectories were driven by gridded meteorological data from the Global Data Assimilation System (GDAS) data, with $1.0^\circ \text{ lat} \times 1.0^\circ \text{ long}$ resolution, 4 times a day (00, 06, 12 e 18 UTC), 23 vertical levels (more information: <http://www.emc.ncep.noaa.gov/modelinfo/index.html>) using a modelled vertical velocity.

3. Data analysis and methodology

The retrieval of the aerosol optical properties is based on the measurements of the aerosol backscatter coefficient (β_{aer}) at 532 nm, up to an altitude of 5–6 km asl. The determination of the vertical profile of the aerosol backscatter coefficient relies on the LIDAR inversion technique following Klett's algorithm, as proposed by Klett (1985) and Fernald (1984), where no multiple-scattering corrections are applied, under the assumption of elastic scattering by spherical aerosols.

In this paper, multiple-scattering effects were not considered, since no low-visibility conditions were taken into account. The valuable information given by depolarization of the incident linearly polarized laser beam is not available in the actual version of the LIDAR system.

This inversion technique is an ill-posed problem in the mathematical sense, leading to errors as large as 30% when applied (Papayannis and Chourdakis, 2002). In general, the inversion of the LIDAR profile is based on the solution of the basic LIDAR equation, taking into account the atmospheric solar background radiation correction (Measures, 1992; Papayannis and Chourdakis, 2002):

$$P(\lambda, R) = P_l \left(\frac{c\tau}{2} \right) \frac{\beta(\lambda, R) A_0 \xi(\lambda) \zeta(R)}{R^2} \exp \left[-2 \int_0^R \alpha(\lambda, r) dr \right] \quad (1)$$

where, $P(\lambda, R)$ is the LIDAR signal received from a distance R at the wavelength λ , P_l is the emitted laser power, A_0 is the telescope receiving area, $\xi(\lambda)$ is the receiver's spectral transmission factor, $\beta(\lambda, R)$ is the atmospheric volume backscatter coefficient, $\zeta(R)$ is the overlap factor between the FOV of the telescope and the laser beam, $\alpha(\lambda, R)$ is the

extinction coefficient, c is the light speed and τ is the laser pulse length.

In Eq. (1), α and β coefficients can be separated into two sets, one for the molecular scattering component and the other for the particle scattering component. Besides, in Klett inversion technique, there is a reference altitude, Z_{ref} , which is used as an upper limit, and has to be an aerosol-free region. Therefore, in this region and above it, the LIDAR signal shows a decay, which follows the molecular contribution only. This is regularly checked using the technique proposed by Chourdakis et al. (2002), in which the LIDAR signal perfectly fits to the signal corresponding to the molecular atmosphere in an aerosol-free region, and thus always assures the perfect alignment of the LIDAR system. In this case the Z_{ref} value was taken in the 8–10 km region, using the technique proposed by (Chourdakis et al., 2002).

To retrieve the aerosol backscatter coefficient, Klett's inversion technique was applied assuming a “guessed” altitude constant extinction-to-backscatter ratio (LR) in the lower troposphere, given by:

$$LR = \frac{\alpha(R)}{\beta(R)}. \quad (2)$$

However, it is known that the LR depends on several parameters, such as the aerosol refractive index, the shape and size distribution of the aerosol particles. Besides, there is a strong dependence of LR on the temperature and humidity profiles in the atmosphere, that might cause variations on the optical parameters of the aerosols (Haanel, 1976), and of course in the presence of turbulence in the atmospheric volume being probed by the LIDAR beam (Stull, 1991).

To derive the appropriate “correct” values of the vertical profile of aerosol backscatter coefficient in the lower troposphere an iterative inversion approach was used (by “tuning” the LR values) based on the inter-comparison of the AOD values derived by LIDAR and CIMEL data, assuming the absence of stratospheric aerosols and that the PBL is homogeneously mixed between ground and 300 m height, where the LIDAR overlap factor is close to 1. Once the “correct” values of the vertical profile of aerosol backscatter coefficient were derived (when the difference of the AODs derived by CIMEL and LIDAR was less than 10%) Klett's method was reapplied, using the appropriate LR values, to retrieve the final values of the vertical profiles of the backscatter and extinction coefficient at 532 nm. It was made a sensitivity analysis of the dependency between the AOD and the LR values, where a variation of about 11% of AOD values in relation to the changes of 10% of the LR values was found.

3.1. CIMEL inversion algorithm

The inversion of the solar radiances measured by the CIMEL sunphotometer to retrieve the AOD values is based on the Beer–Lambert equation, assuming that the contribution of multiple scattering within the small FOV of the sunphotometer is negligible:

$$I_\lambda = I_\lambda^0 \exp \left[- \frac{\tau_\lambda}{\mu_s} \right] \quad (3)$$

where I_{λ}^0 and I_{λ} are the solar irradiances at ground level and at the top of the atmosphere, respectively, and μ_s is the cosine of the solar zenith angle. τ_{λ} is the total atmospheric optical depth from the Rayleigh and aerosol contributions, as well as the ozone and water vapour absorption at 670 nm and 870 nm, respectively, bearing in mind that the ozone contribution is also subtracted from the total optical depth. The AOD at 532 nm was determined by the relation:

$$\frac{\tau_{532}^{aer}}{\tau_{500}^{aer}} = \left(\frac{532}{500}\right)^{-a} \quad (4)$$

where the Ångström Exponent a was derived from the measured optical depth in the blue and red channels (440 nm and 670 nm):

$$a = -\frac{\log\left(\frac{\tau_{440}^{aer}}{\tau_{670}^{aer}}\right)}{\log\left(\frac{440}{670}\right)} \quad (5)$$

The Ångström Exponent is also an indirect mean to retrieve the particle size distribution (Junge, 1963) and its possible composition (Deepak and Gerber, 1983; Almeida et al., 1991). Concerning uncertainty, the major source of error would be in the calibration procedure, which is proportional to the associated uncertainty of the AOD at a given wavelength (Hamonou et al., 1999).

The retrieval of the aerosol size distribution is demonstrated by (Dubovik and King, 2000) and shows that the error of the retrieved volume density $dV(r)/d\ln(r)$ changes as a nonlinear function of particle size, aerosol type, and actual values of the size distribution. The retrieval errors do not exceed 10% for the intermediate particle size range ($0.1 \leq r \leq 7\mu\text{m}$).

4. Results and discussion

The aerosol profiling campaign carried out employed a backscattering LIDAR system in São Paulo, Brazil during July–November of 2007 covering mostly the Southern Hemisphere Dry Season. Trajectory model simulations in conjunction with NOAA-12 hot spots showed that for five days of LIDAR measurements, smoke was advected over São Paulo from different regions with strong fire activity in the Amazonia Region, Brazilian Savannah and Countryside of São Paulo state

(from sugar cane culture). These dates of smoke presence and the main source of particles are presented in Table 1. Additionally to the height ranges of smoke layers (detected by LIDAR system) it shows some optical parameters as the mean LIDAR ratio (LR), the AOD at 532 nm and the mean Ångström Exponent. All these last two parameters represent columnar values; therefore are possibly contaminated by anthropogenic pollution. The values presented in Table 1 are in fair agreement with similar measurements taken in Greece where biomass burning plumes were detected from Russia and Eastern Europe (Amiridis et al., 2005; Amiridis et al., 2009) and in the Korean peninsula (Noh et al., 2008). At Greece the mean value of LR derived at 355 nm found for the period of 2001–2004, was 40 ± 21 sr (Amiridis et al., 2005). The other parameters, namely AOD, AE and LR show some differences which could be attributed to the distinct sites where the observations were made, which reflects a variation in the dominant type of aerosol, micrometeorological and relative humidity effects. The days shown in Table 1 (08/24, 09/07, 09/09, 09/14, 09/15, 10/04 and 10/09) were also observed in MODIS images as biomass burning product transport which are not shown here but are easily retrievable (<http://laadsweb.nascom.nasa.gov/data/search.html>).

Fig. 2 shows ten air masses backtrajectories (in group of five each) incoming into the MASP as shown in the previous cases. The burning sites were identified through NOAA-12 AVHRR sensor taken from (www.cptec.inpe.br/queimadas) during the five day Hysplit backtrajectory. The Hysplit was run backwards from the moment that the smoke layers were detected by the LIDAR system at specific days, heights and times shown in Table 1. The whole 5 day analysis where the burning activity took place, together with the analysis, points out where the main burning locations occurred and its advected plumes go towards São Paulo from the southern part of the Amazon basin and northern Argentina. These events could be identified as long-range transports and in general, to be detected, the plume injection in the source sites has to be into higher altitudes. On the other hand short range transports could be also identified when some burning spots were also observed in SE Brazil probably from sugar cane harvesting related to BB activity (Allen et al., 2004).

The frequency distribution of LR and AE for the 10 cases mentioned in Table 1 is given in Fig. 3a, b, c and d and compared with similar values given by (Cattrall et al., 2005), in which LR and AE frequency are given for many sites scattered around the

Table 1

Dates in 2007 of smoke presence over São Paulo as indicated by the synergy of LIDAR measurements, NOAA-12 hot spots and Hysplit model. The height range of the smoke particle and the Lidar Ratio by the LIDAR system; the mean, AOD and Ångström Exponent by AERONET data and height and time simulated by Hysplit.

Date	Plume layer height range (km)	Final height (km) and time (UTC) simulated by Hysplit	AOD	Ångström Exponent	LR (sr)
30 July	4.5–7.0	5.0–18:00	0.14 ± 0.05	0.85 ± 0.30	75 ± 33
09 August	4.2–5.5	5.0–16:00	0.33 ± 0.10	1.15 ± 0.31	147 ± 68
13 August	5.5–6.0	6.0–16:00	0.22 ± 0.04	1.37 ± 0.11	70 ± 18
24 August	3.5–4.0	4.0–16:00	0.17 ± 0.02	1.31 ± 0.12	49 ± 9
07 September	5.2–9.0	6.0–15:00	0.33 ± 0.10	1.58 ± 0.05	59 ± 14
09 September	2.8–4.0	4.0–15:00	0.41 ± 0.08	1.42 ± 0.09	59 ± 14
14 September	3.2–5.0 and 6.2–8.0	8.0–15:00	0.34 ± 0.06	1.51 ± 0.03	71 ± 19
15 September	3.5–6.0	5.0–18:00	0.42 ± 0.11	1.55 ± 0.04	53 ± 8
04 October	6.5–8.0	5.0–18:00	0.46 ± 0.04	1.20 ± 0.11	55 ± 6
09 October	4.5–6.0	6.0–15:00	0.53 ± 0.20	1.35 ± 0.03	44 ± 16

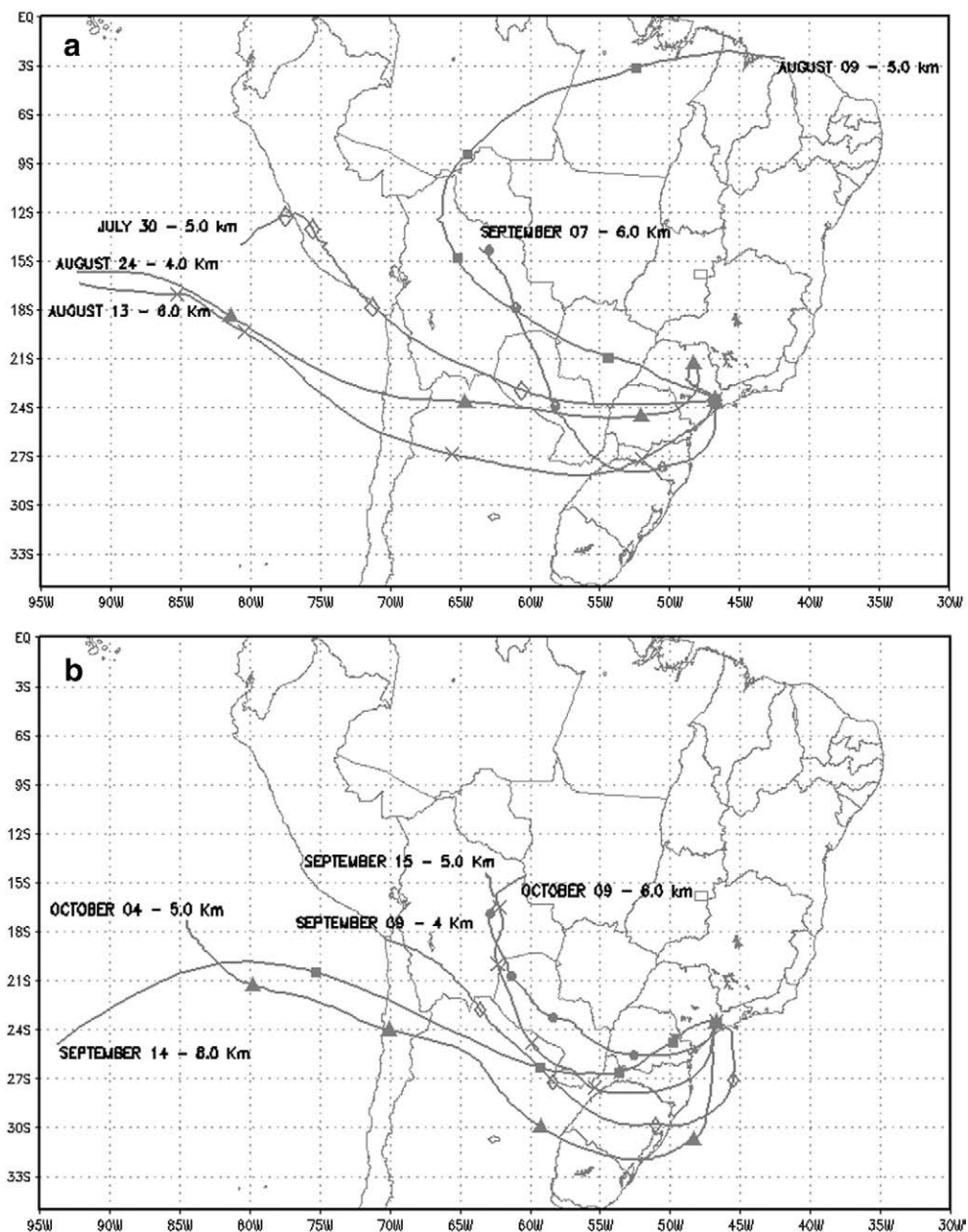


Fig. 2. Backtrajectories from biomass burning detected layer by LIDAR system at São Paulo.

world (Alta Floresta, Brasilia, Cuiaba – Brazil, Los Fieros – Bolivia and Mongu, Senanga and Zambezi – Zambia). The LR distribution shown in Fig. 3a shows a fitted Gaussian centered at around 58.1(9) and its FWHM is 22(2), this is in good agreement with the study by Cattrall et al. (2005), for the BB sites mentioned above. If one takes the fitting of a bi-modal distribution, i.e., the sum of two Gaussians, then the new centroids appear as 55.1(8) and 68.7(16), respectively (Fig. 3b). This strongly suggests an industrial-biomass-burning mixed atmosphere. The same statistical treatment is applied in the case of the AE distributions and the same analysis was carried out, however the agreement is less pronounced. While in our study the fitted Gaussian provided an AE center value of 1.48(2) and

FWHM of 0.39(7); in Cattrall's study these values were 1.8(2). On the other hand if one takes a two-Gaussian fitting instead like the one given in Fig. 3d the new centroids are at 1.42(5) and 1.6 (∞), respectively. This bi-modal approach, again, while bearing some very high uncertainties especially in the second "centroid" estimation, it enlightens the fact that the point with coordinates 1.6 for AE and 28 for frequency is not an outlier but rather a trend in an aerosol mixed atmosphere such as the one present in São Paulo and perturbed by the BB plume transport. The exceedingly high uncertainties are due to the underestimated error bars attributed to the AE values in the fitting process. A more careful analysis concerning these issues lifted in this paper should be in our future studies.

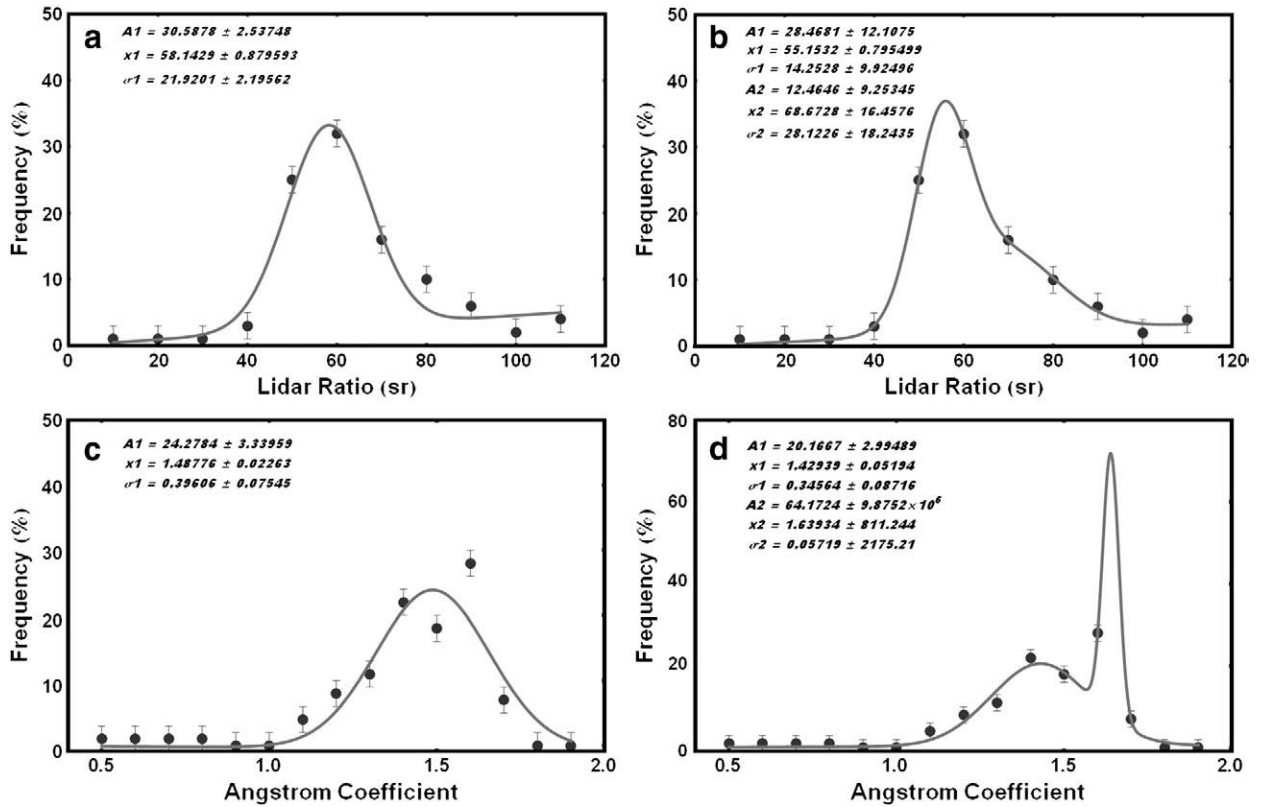


Fig. 3. Gaussian fitting for frequency distribution of LIDAR ratio at 532 nm and the Ångström Exponent. (a) Normal Gaussian fitting for the frequency distribution of the LIDAR ratio at 532 nm. (b) Bi-modal Gaussian fitting for the frequency distribution of the LIDAR ratio at 532 nm. (c) Normal Gaussian fitting for the frequency distribution of the Ångström Exponent. (d) Bi-modal Gaussian fitting for the frequency distribution of the Ångström Exponent.

The daily mean AOD in the period of July–November (corresponding to 182 and 334 Julian days) is depicted in Fig. 4. This plot emphasizes when smoke layers were detected by the LIDAR. The large mean AOD variance given as 0.02 makes it difficult to establish a specific trend for those BB events. One such explanation is that the AOD retrieved by

AERONET is column integrated and the urban aerosols present in the PBL are leading in determining the AOD value. Therefore the presence of biomass burning is not a determining factor easily identifiable in the daily mean AOD in São Paulo as in the case for LR values (Fig. 3a and b). Fig. 5a and b refers to those BB events in the period the LIDAR

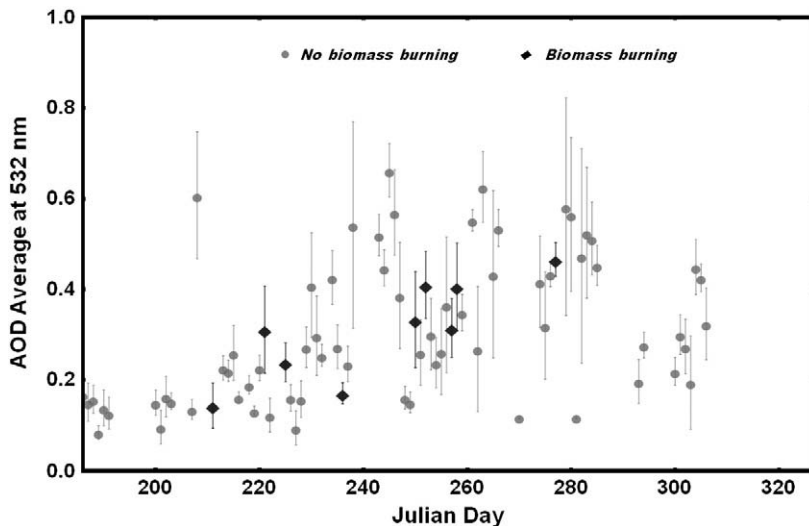


Fig. 4. AOD mean from AERONET data for São Paulo for days with (black) and without (grey) biomass burning during the study period.

campaign was conducted. These two plots are hourly means and put more in evidence the rather high AOD values for São Paulo at 532 nm, corrected by the Ångström Exponent by means of a noninterpolation from the AERONET data.

Fig. 6a and b represents the mean aerosol size distribution in the entire atmosphere (Dubovik and King, 2000) using the AERONET data. Many studies indicate that a bi-modal lognormal function is the most appropriate model for aerosol particle size distributions (e.g.: Remer and Kaufman, 1998; Dubovik et al., 2002; Rodriguez and da Rocha, 2008), similar to the one given in Fig. 6a for the whole period with (10 cases shown at Table 1) and without smoke layer detected by the LIDAR during the campaign period (50 cases) and just for one occurrence involving 2 days with and without smoke layers. One notes that there are no significant differences in the size distribution among those days. In Fig. 6a it is possible to notice that the days without biomass burning obtained a higher mean aerosol distribution mainly in small wavelengths. A possible explanation as previously mentioned is,

for the cases where the PBL is polluted, the AOD as well as the mean aerosol size distribution become higher and there is a decreased contribution of the layers of biomass burning detected over the city. At Greece, free tropospheric particles account on the average for 30% of the total aerosol optical depth, ranging from 5% (clean free troposphere conditions) to 55% (mainly Saharan dust events) (Amiridis et al., 2005).

Noh et al. (2007) display a different pattern for a data set from February 2004 and May 2005 at Korea, where an aerosol layer was detected above the PBL defined as being originated from biomass burning. A maximum peak was found in the fine mode, whereas the coarse mode corresponded to 3 times less the amount of the fine mode. However, values found for AE and LR were very similar to the ones found in São Paulo. This could be corroborated by analyzing Fig. 6b where two consecutive days with biomass burning identification (September 14th and 15th) and without biomass burning identification (September 16th and 18th–September 17th was not available by AERONET) were selected, although

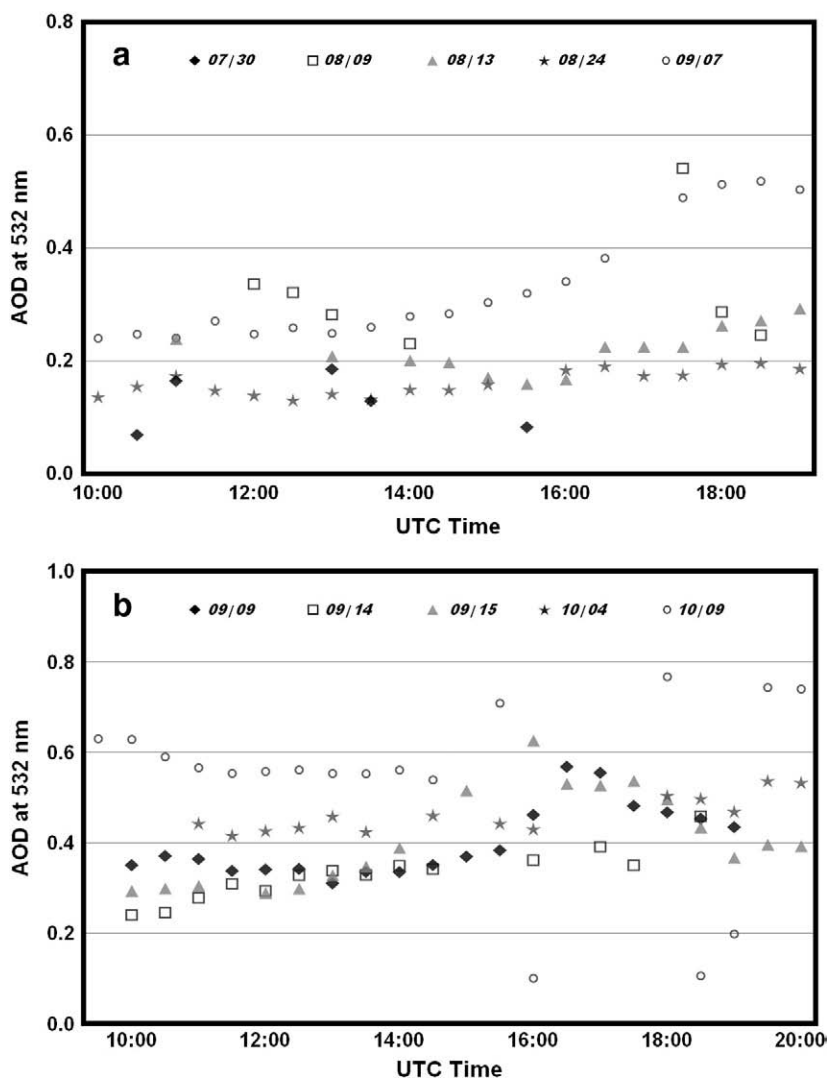


Fig. 5. Hourly AOD at 532 nm in São Paulo from AERONET system for cases with biomass burning detected by the LIDAR system. (a) For July 30, August 09, 13 and 24 and September 07. (b) For September 09, 14, 15 and October 04 and 09.

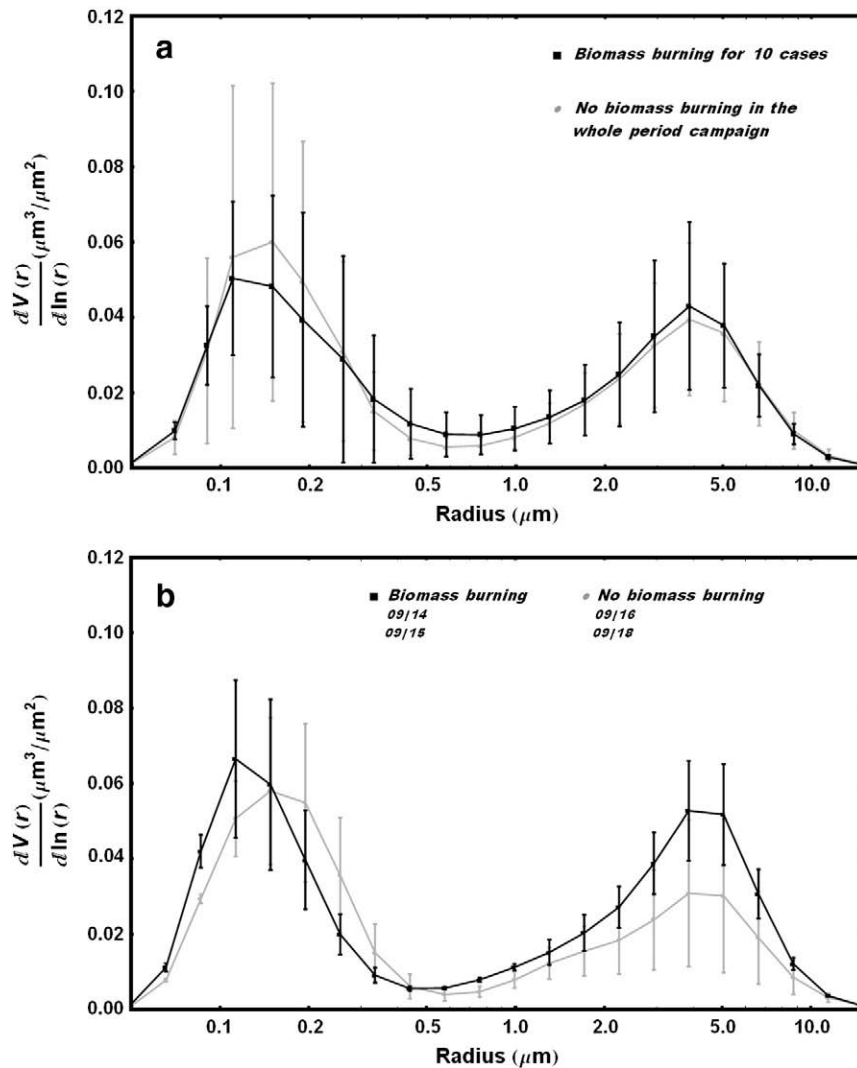


Fig. 6. Mean aerosol size distribution $\frac{dV(r)}{d\ln(r)} (\mu\text{m}^3/\mu\text{m}^2)$ for days with (black) and without (grey) biomass burning detected by the LIDAR system. (a) Complete period campaign. (b) Case with and without biomass burning events, September 14–15th and September 16–18th, respectively.

aerosol load inside the PBL is similar between them (confirmed through LIDAR system detection). It is possible to notice that, despite the high value of standard deviation in both cases, the days with the presence of biomass burning have a higher mean aerosol distribution in all wavelengths as compared to the days without detection.

Data analysis in the meteorological station near to AERONET site shows that this result for this case study also is valid for daily temperature, maximum and minimum temperature (higher for the biomass burning days), as well as for humidity (the opposite) showing that the burning transport from far regions might affect not only the aerosol distribution but also some surface meteorological parameters. However, even the case shown in Fig. 6a does not agree with the one presented by Otero et al. (2004) for a biomass burning case in Argentina. The authors showed a peak in the fine mode, whereas in the case presented here there is a variation both in the fine and coarse modes, without peaks. Possibly, the slight increase in the fine mode would be

related to the entrance of plumes originated from biomass burning, and the increase in the coarse mode is related to particles from the surface. Then it is possible to notice that no significant difference was found.

Fig. 7 shows the Angström Exponent as a function of the aerosol optical depth for the complete data and cases previously selected at São Paulo, the grey filled lines are the AOD and AE median values for all data and the dashed lines are the respective median standard deviation. The AE values below the horizontal line corresponding to the median, $AE = 1.45(10)$, are an indication that most of the aerosols load is in the coarse mode size distribution. Those values above the median line belong to the fine mode size type of aerosols. The AE indicates a small sized particle distribution similar to those found in the presence of biomass burning aerosols as shown by Kaskaoutis et al. (2007), in Alta Floresta, Brazil. Making the same interpretation to the AOD median vertical line, $AOD = 0.167(54)$, the values in the left side of the AOD median corresponding to low extinction and

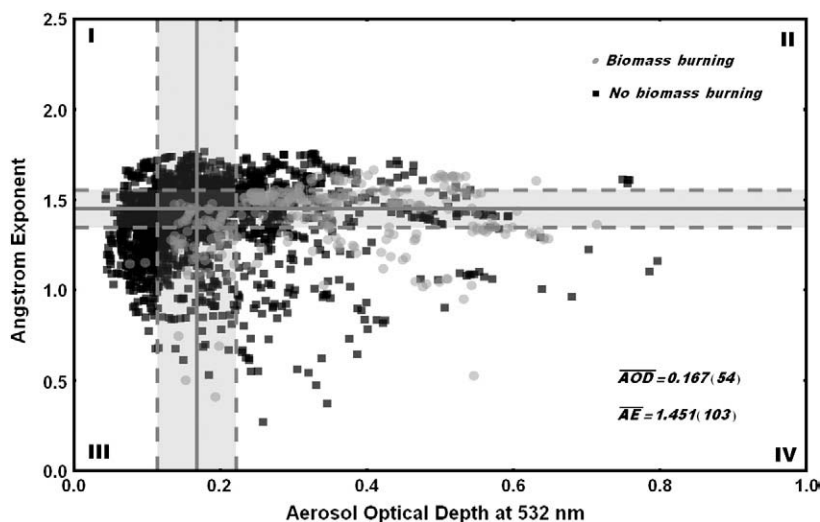


Fig. 7. Ångström Exponent versus aerosol optical depth at 532 nm for the 10 cases selected and for the complete period of the study. The four distinctive sectors represent different types and sizes of aerosol according to the AOD and AE values.

absorption of radiation aerosol types, and the right side is related to the high extinction and absorption radiation types. The median values were assumed once the AE vs. AOD distribution is rather asymmetrical (Landulfo and Lopes, 2009). The plot was divided into four distinctive sectors, I, II, III and IV. Each of them represents different types and sizes of aerosol according to the AOD and AE values. This paper should be focusing mainly on regions II and IV, that correspond to fine mode size distribution and high absorption (extinction) aerosol types, and coarse mode and high absorption (extinction) aerosol types, respectively. In sector II there is a strong indication of the predominance of biomass burning aerosols in the atmosphere as the large AE corresponds to small sized particles and the large AOD for a strong absorbing type of aerosols. The same reasoning can be applied to sector IV, although the values below the AE median values can be associated to particle growth during the long-range transport (Müller et al., 2007).

4.1. 07 September 2007 – case study

The period which comprised the day analyzed was marked by the predominance of an intense anticyclonic circulation in the low troposphere that contributed for the decrease in precipitation and relative humidity in most parts of Brazil (CLIMANÁLISE, Boletim de monitoramento e análise climática, 2007). In Fig. 8a it is possible to observe fine aerosol layers around 5 and 6 km height along almost all the data period for September 7th, 2007. It is also possible to notice the growth of the atmospheric boundary layer throughout the day with the presence of at least two cloud detections (at about 15:00 and 19:00 UTC). As a contrast, it is shown in Fig. 8b the range corrected LIDAR signal for a clean atmosphere day without the presence of biomass burning layers for September 3, 2007. The aerosol backscatter profiles taken between 13:17 and 21:05 UTC, on 07 September 2007 are shown in Fig. 9. An aerosol layer is present below 2500 m that originated from urban aerosol. It is also noticed that aerosol layers at around 5000–6500 m which is an indication

of the presence of long-range transported particles in the free troposphere originate from remote areas.

To identify the source of high aerosol loadings observed over São Paulo region during this day, air mass back trajectory analysis in 6 km at 15:00 UTC was performed with conjunction with satellite data derived from the NOAA-12 sensor as it can be seen in Fig. 10. According to this figure, the air mass from Central South America region and the intense aerosol layers observed in this day in free atmosphere could be therefore attributed to long-range transported BBA by active fires (8700 hot spots during these 5 days) and was advected to the MASP.

The Ångström Exponent value obtained for this day was found to be 1.58 ± 0.05 indicating the presence of rather small aerosol particles, such carbonaceous particles or even smoke aged aerosols diluted over the urban area of São Paulo (Eck et al., 1999). If the assumption of a well-mixed boundary layer in the first 300 m is included and matches the LIDAR and CIMEL AOD values, a mean LR of the order of 59 sr is found. The mean AOD derived values from the CIMEL data at 532 nm on 07 September 2007, were quite low, of the order of 0.33. Analyzing Fig. 11 it can be seen that there is a higher amount of fine aerosols, as compared to the coarse mode (approximately twice), possibly due to the entrance of burning plumes in the free atmosphere.

5. Conclusions

In this study 10 cases were selected between July–November 2007, where layers with highly absorbent material were detected by the LIDAR system installed in São Paulo, Brazil. Trajectory model simulations showed that for until five days from LIDAR measurements, air masses were advected from different regions of South America with intensive biomass burning activities.

The synergy of LIDAR, sunphotometer measurements, MODIS images and modelling allowed having the confirmation and estimate key optical characteristics of the aerosols observed during these events. These results are important for

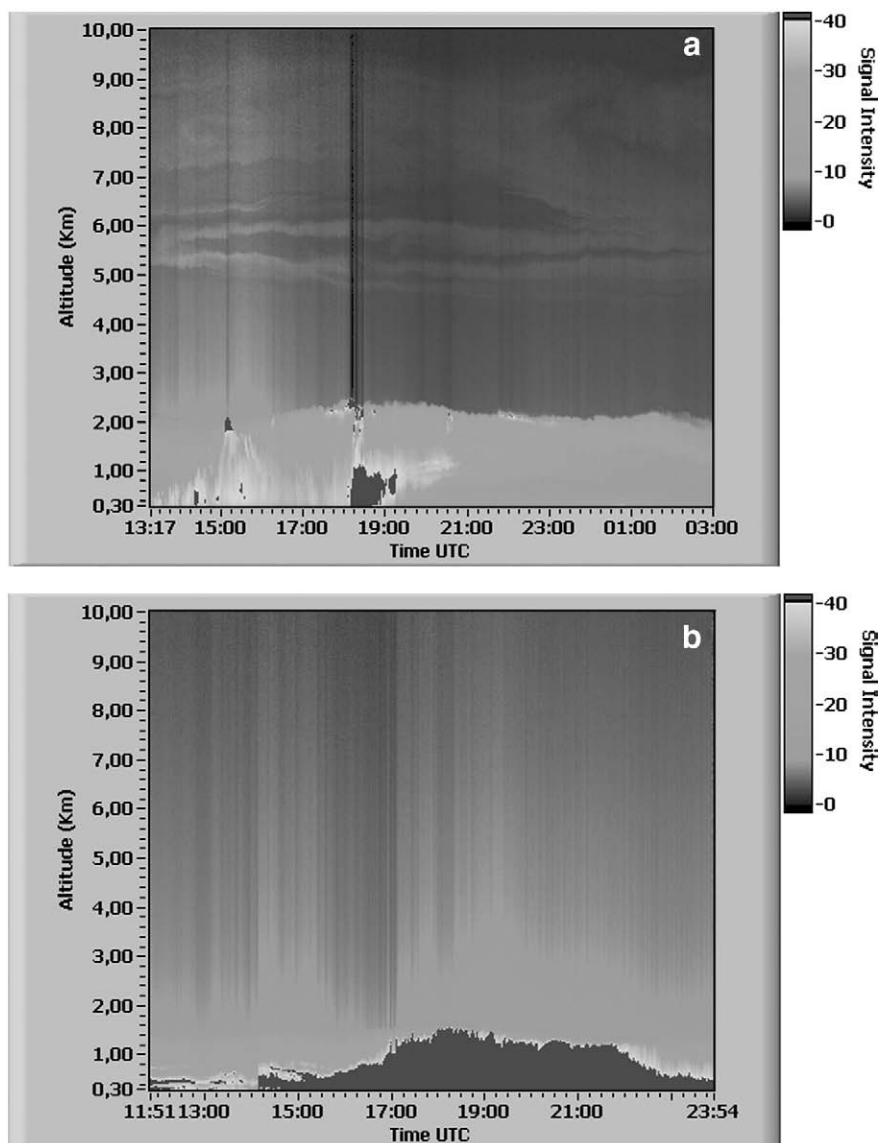


Fig. 8. LIDAR range corrected signal (a) measurements on September 07, 2007. It provides the visualization of the atmospheric boundary layer and the long-range transporting biomass burning layer. (b) Measurement on September 03, 2007. It provides the visualization of the atmospheric boundary layer and the clear free atmosphere.

radiative forcing studies in the area (Balis et al., 2003) and climatic studies due to the increasing on biomass burning during the last decade (Amiridis et al., 2009). The Klett inversion technique was applied in an iterative mode, with the synergy of the CIMEL data. Using this synergetic approach a matched LIDAR ratio (LR) at 532 nm for each case of aerosol LIDAR profiles during the dry season was derived.

The five-day air mass backtrajectories together with active fires (and in some cases MODIS images) confirmed the origin of this material for 10 cases selected through LIDAR measurements being a resultant of biomass burning. The main regions from where air masses with biomass burning material were advected to the city of São Paulo were identified: south of the Amazon basin, north of Argentina and countryside of state of São Paulo. The mean AOD was

between 0.14 and 0.53 (integrated column) whereas the LR and AE varied between 44–147 sr and 0.85–1.58 respectively for the days where plume entrance was detected, which is quite similar to the one found on biomass burning cases by Amiridis et al. (2009). The analysis of the frequency distribution agreed with the possibility that the resulting material comes from biomass burning, as compared with Catrall et al. (2005).

The AOD analysis conducted in the whole period shows that the plume onset in the São Paulo region does not change drastically the daily AOD mean values compared with the days with and without biomass burning layers. However, when the LIDAR data are taken into account it is possible to realize the time the plume onset takes place. The aerosol size distribution has shown little variation when the days with

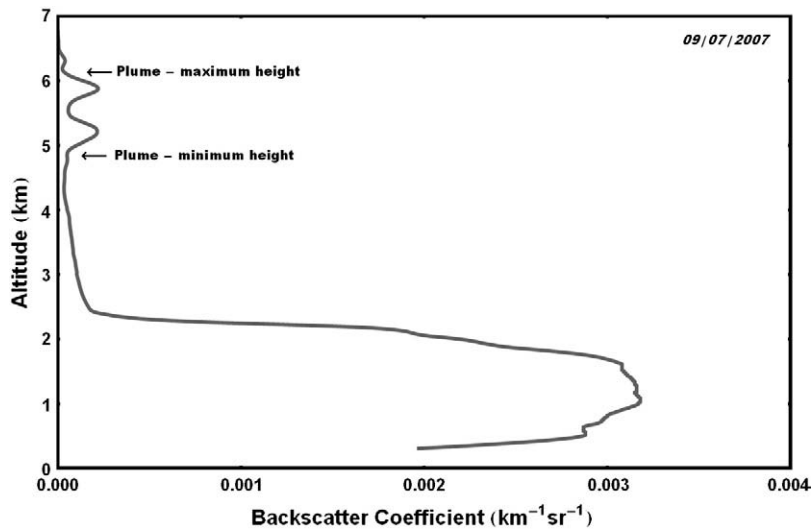


Fig. 9. Aerosol backscatter coefficient at 532 nm on 07 September 2007 (13:17–21:05 UTC). The aerosol backscattering coefficient provides an alternative way to visualizing the biomass burning layers present in the free atmosphere.

and without plumes are considered, whereas more attention should be taken to the size distribution inside the PBL rather than in the free atmosphere.

In a case study presented the methodology to determine the heights of the plumes in the free atmosphere through the

backscatter coefficient profile and the difference between the LIDAR signal intensity on days with and without detection of biomass burning plumes on the city of São Paulo was shown.

The great importance to stress in the detection of these biomass burning plumes is that despite the small impact both in

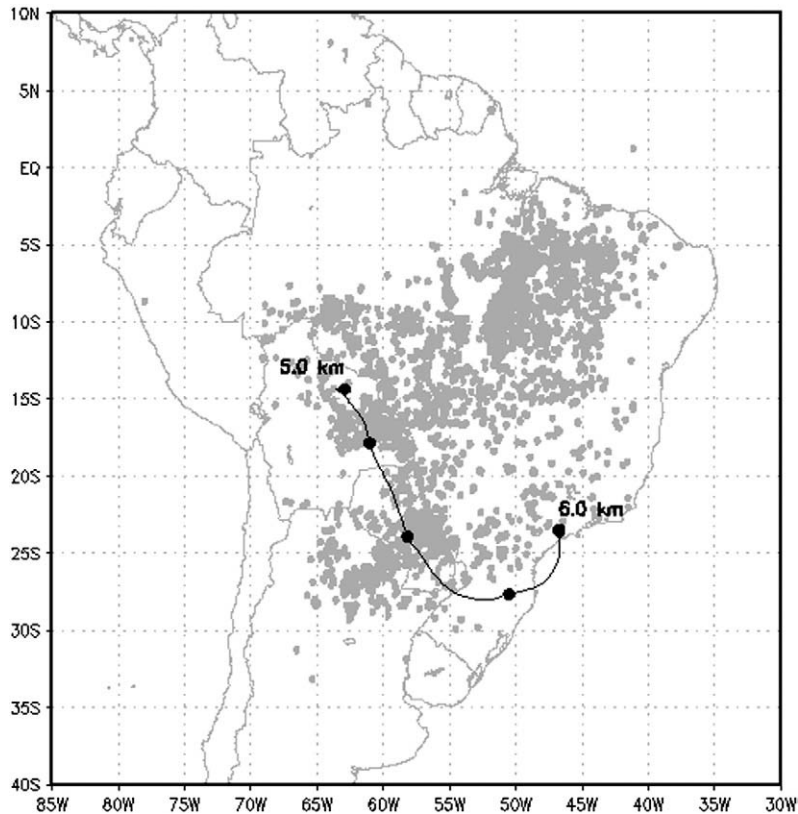


Fig. 10. Five-day backtrajectory from Hysplit model and active fires in 07 September 2007.

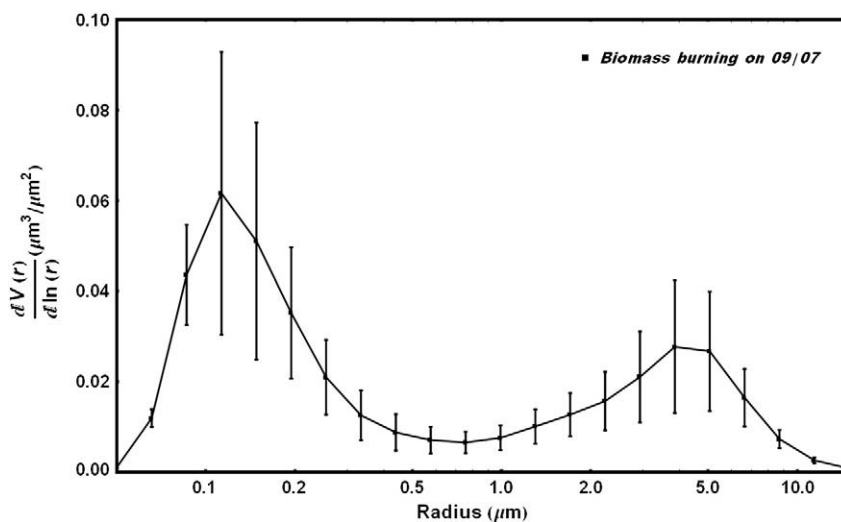


Fig. 11. Mean aerosol distribution $\frac{dV(r)}{d\ln(r)}$ ($\mu\text{m}^3/\mu\text{m}^2$) for a biomass burning event on September 07, 2007.

the AOD and AE, it is possible to notice these entrances in LR values. In such case, added to the high urban pollution in the city of São Paulo is the pollution coming from biomass burning of several regions in South America, which play a very important role in the global aerosol budget over this region.

Acknowledgements

The authors would like to thank the supporting agencies Conselho Nacional de Desenvolvimento e Pesquisa (CNPq), Comissão Nacional de Energia Nuclear (CNEN), and Fundação de Amparo Pesquisa do Estado de São Paulo for financing the research being carried at the institutes involved in this study. The authors acknowledge the NASA AERONET Project and team members (Dr. Paulo Artaxo for maintaining the AERONET database at São Paulo, Brazil) for their contribution in providing and maintaining the Cimel sunphotometers. The CIMEL data were provided by the AERONET network and the MODIS data were provided by ESA-NASA. The MODIS data used to confirmation in this study were acquired as part of the NASA's Earth Science Enterprise.

References

- Allen, A.G., Cardoso, A.A., Rocha, G.O.D., 2004. Influence of sugar cane burning on aerosol soluble ion composition in southeastern Brazil. *Atmospheric Environment* 38, 5025–5038.
- Almeida, G.A.D., Koepke, P., Shettle, E.P., 1991. *Atmospheric Aerosols*, Global Climatology and Radiative Characteristics. Deepak Publishers, Hampton, VA.
- Amiridis, V., Balis, D.S., Kazadzis, S., Bais, A., Giannakaki, E., Papayannis, A., Zerefos, C., 2005. Four-year aerosol observations with a Raman lidar at Thessaloniki, Greece, in the framework of European Aerosol Research Lidar Network (EARLINET). *Journal of Geophysical Research* D21203, 827–849.
- Amiridis, V., Balis, D.S., Giannakaki, E., Stohl, A., Kazadzis, S., Koukoulis, M.E., Zanis, P., 2009. Optical characteristics of biomass burning aerosols over southeastern Europe determined from UV–Raman lidar measurements. *Atmospheric Chemistry and Physics* 9, 2431–2440.
- Andreae, M.O., Rosenfeld, D., Artaxo, P., Costa, A.A., Frank, G.P., Longo, K.M., Silva-Dias, M.A.F., 2004. Smoking rain clouds over the Amazon. *Science* 303, 1337–1342.
- Balis, D., Papayannis, A., Galani, E., Marengo, F., Santacesaria, V., Hamonou, E., Chazette, P., Zerefos, I.Z.C., 2000. Tropospheric lidar aerosol measurements and sun photometric observations at Thessaloniki, Greece. *Atmospheric Environment* 34, 925–932.
- Balis, D.S., Amiridis, V., Zerefos, C., Gerasopoulos, E., Andreae, M., Zanis, P., Kazantzidis, A., Kazadzis, S., Papayannis, A., 2003. Raman lidar and sunphotometric measurements of aerosol optical properties over Thessaloniki, Greece during a biomass burning episode. *Atmospheric Environment* 37, 4529–4538.
- Basart, S., Perez, C., Cuevas, E., Baldasano, J.M., Gobbi, G.P., 2009. Aerosol characterization in Northern Africa, Northeastern Atlantic, Mediterranean Basin and Middle East from direct-sun AERONET observations. *Atmospheric Chemistry and Physics Discussions* (9) 7707–7745.
- Boian, C., Kirchhoff, V.W.J.H., 2004. Measurements of CO in an aircraft experiment and their correlation with biomass burning and air mass origin in South America. *Atmospheric Environment* 38, 6337–6347.
- Cattrall, C., Reagan, J., Thome, K., Dubovik, O., 2005. Variability of aerosol and spectral lidar and backscatter and extinction ratios of key aerosol types derived from selected Aerosol Robotic Network locations. *Journal of Geophysical Research* 110, D10S11.
- Chourdakis, G., Papayannis, A., Porteneuve, J., 2002. Analysis of the receiver response for a non-coaxial lidar system with fiber-optic output. *Applied Optics* 41, 2715–2723.
- Clemesha, B.R., Rodrigues, S.N., 1971. Stratospheric scattering profile at 23 degrees south. *Journal of Atmospheric and Solar-Terrestrial Physics* 33, 1119–1125.
- CLIMANÁLISE, Boletim de monitoramento e análise climática. Número 22.
- Crum, T.D., Stull, R.B., Eloranta, E., 1987. Coincident lidar and aircraft observations of entrainment into thermals and mixed layer. *Journal of Climate and Applied Meteorology* 26, 774–788.
- Crutzen, P.J., Andreae, M.O., 1990. Biomass burning in the tropics: impact on atmospheric chemistry and biogeochemical cycles. *Science* 250, 1669–1678.
- Deepak, A., Gerber, H.E., 1983. *Aerosols and their climate effects*. Series Report 55. International Council of Scientific Unions and WMO, Switzerland.
- Dias, M.A.F.S., Artaxo, P., Andreae, M.O., 2004. Aerosols impact clouds in the Amazon basin. *GEWEX Newsletter* 14, 4–6.
- Draxler, R.R., Hess, G.D., Description of the HYSPLIT_4 Modelling System, Technical Report, NOAA Tech. Mem. ERL ARL-224, 1997.
- Dubovik, O., King, M.D., 2000. A flexible inversion algorithm for retrieval of aerosol optical properties from sun and sky radiance measurements. *Journal of Geophysical Research* 105, 20673–20696.
- Dubovik, O., Holben, B., Eck, T., Smirnov, A., Kaufman, Y., King, M., Tanre, D., Slutsker, I., 2002. Variability of absorption and optical properties of key aerosol types observed in worldwide locations. *Journal of Atmospheric Sciences* 59, 590–608.
- Eck, T.F., Holben, B.N., Reid, J.S., Dubovik, O., Smirnov, A., O'Neill, N.T., Slutsker, I., Kinne, S., 1999. Wavelength dependence of the optical depth of biomass burning, urban, and desert dust aerosols. *Journal of Geophysical Research* 104, 31333–31349.
- Fernald, G.F., 1984. Analysis of atmospheric lidar observations: some comments. *Applied Optics* 23, 652–653.
- Ferrare, R.A., Schols, J.L., Eloranta, E.W., 1991. Lidar observations of banded convection during BLX83. *Journal of Applied Meteorology* 30, 312–326.

- Freitas, S.R., Longo, K.M., Dias, M.A.F.S., Artaxo, P., 1996. Numerical modeling of air mass trajectories from the biomass burning areas of the amazon basin. *Anais da Academia Brasileira de Ciências* 68, 1.
- Gassmann, M.I., Pérez, C.L., 2006. Trajectories associated to regional and extra-regional pollen transport in the southeast of Buenos Aires province, Mar del Plata. Argentina, *International Journal of Biometeorology* 50, 280–291.
- Gobbi, G.P., Kaufman, Y.J., Koren, I., Eck, T.F., 2007. Classification of aerosol properties derived from AERONET direct sun data. *Atmospheric Chemistry and Physics* 7, 453–458.
- Haanel, G., 1976. The properties of atmospheric aerosol particles in function of the relative humidity at thermodynamic equilibrium with the scattering moist air. *Advances in Geophysics* 19, 73–188.
- Hamonou, E., Chazette, P., Balis, D., Dulac, F., Scheneider, X., Galani, E., Ancellet, G., Papayannis, A., 1999. Characterization of the vertical structure of Saharan dust export to the Mediterranean basin. *Journal of Geophysical Research* 104, 22257–22270.
- Holben, B.N., Eck, T.F., Slutsker, I., Tanré, D., nd A Setzer, J.P.B., Vermote, E., Reagan, J.A., Kaufman, Y.J., Nakajima, T., Lavenu, F., Jankowiak, I., Smirnov, A., 1998. Aeronet – a federated instrument network and data archive for aerosol characterization. *Remote Sensing of the Environment* 66, 1–16.
- IPCC, Intergovernmental Panel on Climate Change 2001: The third assessment report to the intergovernmental panel on climate change, Technical Report, Cambridge, New York, 2001.
- IPCC, Intergovernmental Panel on Climate Change 2007: The Fourth assessment report to the intergovernmental panel on climate change, Technical Report, Cambridge, New York, 2007.
- Junge, C.E., 1963. *Air Chemistry and Radioactivity*, 3rd edition. Academic Press, New York.
- Kaskaoutis, D., Kambezidis, H., Hatzianastassiou, N., Kosmopoulos, P., Badarinath, K., 2007. Aerosol climatology: on the discrimination of aerosol types over four AERONET sites. *Atmospheric Chemistry and Physics Discussions* 7, 6357–6411.
- Kaufman, Y.J., Tanré, D., Algorithm for remote sensing of tropospheric aerosol from MODIS, Technical Report, NASA/GSFC, 1998.
- Kaufman, Y.J., Tanré, D., Boucher, O., 2002. A satellite view of aerosols in the climate system. *Nature* 419, 215–223.
- Klett, J.D., 1985. Inversion with variable backscatter/extinction ratios. *Applied Optics* 11, 1638–1643.
- Landulfo, E., Lopes, F.J.S., 2009. Initial approach in biomass burning aerosol transport tracking with calipso and modis satellites, sunphotometer and a backscatter lidar system in brazil. *Proceedings of SPIE – The International Society for Optical Engineering* 7479, 747905.
- Landulfo, E., Papayannis, A., Artaxo, P., Castanho, A.D.A., Freitas, A.Z., Souza, R.F., Junior, N.D.V., Jorge, M.P.M.P., Sánchez-Ccoylo, O.R., Moreira, D.S., 2003. Synergetic measurements of aerosols over São Paulo, Brazil using lidar, sunphotometer and satellite data during dry season. *Atmospheric Chemistry and Physics* 3, 1523–1539.
- Landulfo, E., Papayannis, A., Souza, R.F., Freitas, A.Z., Lidar aerosol profile categorisation in São Paulo, Brazil, Reviewed and revised papers presented at the 22nd International Laser Radar Conference 1 (2004) 499–502.
- Landulfo, E., Papayannis, A., de Freitas, A.Z., Jr, N.D.V., Souza, R.F., Gonçalves, A., Castanho, A.D.A., Artaxo, P., Sánchez-Ccoylo, O.R., Moreira, D.S., Jorge, M.P.M.P., 2005. Tropospheric aerosol observations in São Paulo, Brazil using a compact lidar system. *International Journal of Remote Sensing* 36, 2797–2816.
- Lara, L.B.L.S., Artaxo, P., Martinelli, L.A., Victoria, R.L., Camargo, P.B., Krusche, A., Ayers, G.P., Ferraz, E.S.B., Ballester, M.V., 2001. Chemical composition of rainwater and anthropogenic influences in the Piracicaba river basin southeast Brazil. *Atmospheric Environment* 35, 4937–4945.
- Lara, L.L., Artaxo, P., Martinelli, L.A., Camargo, P.B., Victoria, R.L., Victoria, E.S.B., 2005. Properties of aerosol from sugar-cane burning emissions in southeastern Brazil. *Atmospheric Environment* 39, 4627–4637.
- Longo, K., Thompson, A.M., Kirchoff, V.W.J.H., Remer, L.A., Freitas, S.R., Dias, M.A.F.S., Artaxo, P., Hart, W., Spinhirne, J.D., Yamasoe, M.A., 1998. Correlation between smoke and tropospheric ozone concentrations in Cuiabá during SCAR-B. *Journal of Geophysical Research* 104, 12113–12129.
- McGowan, H., Clark, A., 2008. Identification of dust transport pathways from Lake Eyre, Australia using Hysplit. *Atmospheric Environment* 42, 6915–6925.
- Measures, R.M., 1992. In laser remote sensing fundamentals and applications. Krieger Publishing Company.
- Mel, S.H., Spinhirne, J.D., Chou, S.H., Palm, S.P., 1985. Lidar observations of vertically organized convection in the planetary boundary layer over the ocean. *Journal of Climate and Applied Meteorology* 24, 806–821.
- Müller, D., Ansmann, A., Mattis, I., Tesche, M., Wandinger, U., Althausen, D., Pisani, G., 2007. Aerosol-type-dependent lidar ratios observed with raman lidar. *Journal of Geophysical Research* 112, D16202.
- Noh, Y.M., Kym, Y.J., Choi, B.C., Murayama, T., 2007. Aerosol lidar ratio characteristics measured by a multi-wavelength Raman lidar system at Anmyeon Island. *Atmospheric Research* 86, 76–87.
- Noh, Y.M., Kim, Y.J., Muller, D., 2008. Seasonal characteristics of lidar ratios measured with a Raman lidar at Gwangju. Korea in Spring and Autumn, *Atmospheric Environment* 42, 2208–2224.
- Otero, L., Ristori, P., Holben, B., Quel, E., 2004. Detection of biomass burning aerosols in Córdoba, Argentina, using the Aeronet/NASA data base. *Óptica pura y Aplicada* 37.
- Papayannis, A., Chourdakis, G., 2002. The EOLE Project. A multi-wavelength laser remote sensing (Lidar) system for ozone and aerosol measurements in the troposphere and the lower stratosphere. Part ii: aerosol measurements over Athens, Greece. *International Journal of Remote Sensing* 23, 179–196.
- Reid, J.S., Koppmann, R., Eck, T.F., Eleuterio, D.P., 2005a. A review of biomass burning emissions part ii: intensive physical properties of biomass burning particles. *Atmospheric Chemistry and Physics* 5, 799–825.
- Reid, J.S., Eck, T.F., Christopher, S.A., Koppmann, R., Dubovik, O., Eleuterio, D.P., Holben, B.N., Reid, E.A., Zhang, J., 2005b. A review of biomass burning emissions part iii: intensive optical properties of biomass burning particles. *Atmospheric Chemistry and Physics* 5, 827–849.
- Remer, L.A., Kaufman, Y.J., 1998. Dynamic aerosol model: urban/industrial aerosol. *Journal of Geophysical Research* 103, 13859–13871.
- Rodriguez, C., da Rocha, R., 2008. Does the pollution affect the development of thunderstorms in the city of São Paulo?, in: *International Conference on Grounding and Earthing & 3rd International Conference on Lightning Physics and Effects*, pp. 306–310.
- Rosenfeld, D., 2000. Suppression of rain and snow by urban and industrial air pollution. *Science* 287, 1793–1796.
- Stull, R.B., 1991. *An Introduction to Boundary Layer Meteorology*, 2nd edition. Kluwer Academic, Boston.
- Vana, M., Tamm, E., 2002. Propagation of atmospheric aerosol and the area of representativeness of its measurements in the Baltic Sea region. *Atmospheric Environment* 36, 391–401.
- Yamasoe, M.A., Kaufman, Y.J., Dubovik, O., Remer, L.A., Holben, B.N., Artaxo, P., 1998. Retrieval of the real part of the refractive index of aerosols from sun/sky radiometers during scar-b. *Journal of Geophysical Research* 103, 31893–31902.
- Yamasoe, M.A., Artaxo, P., Miguel, A.H., Allen, A.G., 2000. Chemical composition of aerosols particles from direct emissions of vegetation fires in the amazon basin: watersoluble species and trace elements. *Atmospheric Environment* 34, 1641–1653.
- Yamasoe, M.A., Randow, C.V., Manzi, A.O., Schafer, J.S., Eck, T.F., Holben, B.N., 2006. Effect of smoke and clouds on the transmissivity of photosynthetically active radiation inside the canopy. *Atmospheric Chemistry and Physics* 6, 1645–1656.